Arabian Journal for Science and Engineering (2019) 44:1569–1581
https://doi.org/10.1007/s13369-018-3621-4

RESEARCH ARTICLE - MECHANICAL ENGINEERING

Ageing Behaviour of Sc-Doped Cu–Zn–Al Shape Memory Alloys

Gourab Saha[1,2,3] · Manojit Ghosh[2] · Ajesh Antony[3] · Koushik Biswas[4]

Received: 19 March 2018 / Accepted: 25 October 2018 / Published online: 9 November 2018

Abstract
The effect of scandium (Sc), when added in trace, on the ageing behaviour of Cu–Zn–Al shape memory alloy was investigated in the present work. Cu–Zn–Al shape memory alloy was prepared by melting 70:30 brass using commercial grade Cu strips and Al chips. Sc was added using Al–Sc 2 wt% master alloy at the time of melting, and the final composition was adjusted to 0.1 wt% Sc. Chemical composition of the alloys was analysed by using EDAX and spectrometer. The influence of Sc on mechanical properties under different ageing conditions were primarily evaluated by Vickers hardness test. Optical and scanning electron microscopy (SEM) was used to analyse the microstructure. Differential scanning calorimetry was used to measure the transformation temperatures, correspond to martensite to austenite or the reverse transformation. Thermo-Calc software was used to construct a phase fraction diagram as a function of temperature to obtain the evolving phases during quenching and subsequent ageing process for both of the alloy systems. The ageing behaviour was also examined using XRD and SEM characterization and explained in the light of phase predictions obtained from the thermodynamic calculations. Subsequently, transmission electron microscopy investigation was carried out to evaluate the influence of Sc on the size and habit planes of the precipitates in Cu–Zn–Al ternary alloy system. Sc has been found to reduce the transformation temperature and consequently increase the mobility of the martensite/austenite interface.

Keywords Shape memory alloys · Sc addition · Ageing · Microhardness · Precipitates

1 Introduction

Shape memory alloys (SMAs) exhibit unique thermo-mechanical properties due to diffusionless and reversible thermoelastic martensitic transformation aided by stress and/or temperature. This transformation is responsible for the macroscopic shape change in SMAs through a special training process that includes a thermo-mechanical cycle through the transformation region [1]. Austenite (β phase) is the parent phase for this transformation [2,3].

Among numerous SMAs, Cu-based alloys earned significant importance during recent past due to the low production cost, good memory properties, easy fabrication, better electrical and thermal conductivity [1,2,4,5]. The combination of above properties makes Cu–Zn–Al alloys a commercially exploited material for shape memory applications. However, the Cu–Zn–Al SMAs reportedly [5] show modest shape memory properties (maximum recoverable strain up to 4%) along with stabilization of martensitic phase [5] compared to other SMAs [6]. The proposed mechanism of martensitic stability includes changes in chemical and topological characteristics that resemble the attributes of isothermal ageing [7]. Due to repetitive transformation cycle, generation of precipitates that interferes hysteresis loop profile and subsequently two-way shape memory effect through pinning of the migrating interphase boundaries restricting grain growth [8]. To improve the SMA performance, attention has been paid on composition differences with varying quantities. Grain refinement also contributed to a significant improvement in SMA properties by restricting grain growths and providing potential sites for strain release [9]. Investigations revealed [10] that minute variation in chemistry may signif-

✉ Manojit Ghosh
manojit_ghosh1@rediffmail.com

1 Materials Science, Tampere Wear Center, Tampere University of Technology, Tampere, Finland

2 Department of Metallurgy and Materials Engineering, Indian Institute of Engineering Science and Technology, Shibpur, Howrah 711 103, India

3 Institute for Frontier Materials, Deakin University, Geelong Waurn Ponds Campus, Geelong, Australia

4 Department of Metallurgical and Materials Engineering, Indian Institute of Technology, Kharagpur 721302, India

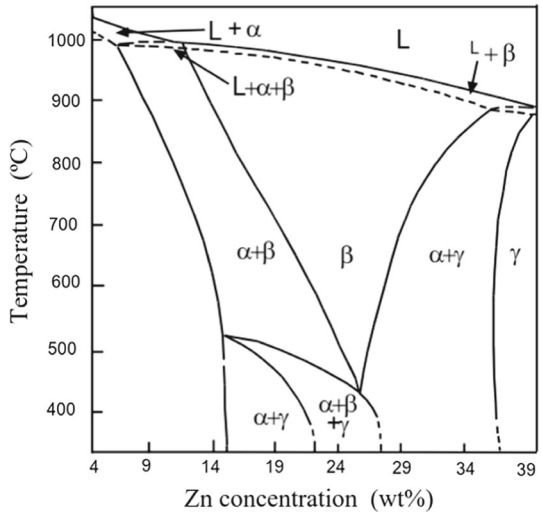

Fig. 1 Vertical cross section of Cu–Zn–Al ternary phase diagram with 6 wt%Al [11]

icantly change shape memory effect (SME) by influencing habit plane variants (HPV), lattice invariant shear (LIS), self-accommodation (SA), etc.

Figure 1 represents the vertical section of the Cu–Zn–Al ternary equilibrium phase diagram at 6 wt% Al content [11]. The area of interest is the high-temperature β phase manifested by disordered BCC structure, when quenched to ambient temperature, transforms into an ordered B2 or DO_3 phase [12]. Further cooling of the alloy may result into martensitic phase. Nevertheless, other than cooling, the transformation is also dependent on the alloy composition [12]. On enhancing the Al content, the β phase decomposes into primary solid solution of Cu (α phase) and cubic Cu_5Zn_8 phase (γ) at 700 K. The β phase in the binary Cu–Al system transforms to martensite when quenched to ambient temperature, but on slow cooling it decomposes into eutectoid compositions of α and Cu_9Al_4 cubic phases (γ_2) at 838 K [12]. Thus, it is apparent that higher Al content reduces tendency of martensitic transformation due to the susceptibility of Cu_9Al_4 cubic phase (γ_2) precipitation [12]. Hence, ternary elements Ni or Zn are added to stabilize the β phase suppressing the diffusion of Cu and Al atoms. The brief discussion so far reveals that the Cu–Zn–Al alloy that can be used as SMA should have the composition in the range of Cu–(10–30)wt%Zn–(5–10)wt%Al so as to achieve a high-temperature β phase [13].

It is also pertinent to mention that that shape memory properties of the Cu alloys depend on the parent austenitic and product martensitic phases. Since Cu-based alloys are highly sensitive to the low-temperature ageing effects, deeper understanding for temperature-dependent applications is required. Parent phase stabilization had been attributed to the inadequate ordering and precipitate formation during quenching process [14]. Previously published reports indicate that parent phase stabilization is less likely for the Cu-based shape memory alloys in contrast to the martensitic phase stabilization [15]. The martensitic stability occurs due to the excess quenched-in vacancies, formed during quenching and rise of A_s and A_f temperatures are the indicators of the martensite stability. The quenched-in vacancies and/or precipitates cause pinning of interfaces between parent and martensite phases and/or martensite variant boundaries resulting in a martensitic stabilization [15], the supportive mechanisms are considerably reviewed in [16–18]. Metallurgical factors, for example, grain size, alloy composition, lattice defects, and heat treatments affect stabilization. Lower grain size offers higher grain boundaries which act as sinks for vacancies. Similar effects can be seen in case of lattice defects also. Methods of reducing the excess vacancies are the adopted principles to reduce the stabilization. Step quenching, hot rolling, thermal cycling introduces dislocations which act as sinks for the vacancies. Precipitates also lock the dislocations and allow annihilation of the quenched-in-vacancies, reducing the martensite stability [15].

Realizing the importance of the role of precipitates several attempts were made using elements like Ti, Zr, V, Pb, B [7,9,19–22] in the case of Cu–Al–Ni and Cu–Zn–Al systems. Bhuniya et al [9] worked on the ageing of Cu–Zn–Al-based alloy and found that microstructural evolution at the peak aged condition degrades the shape memory effect. Tracer additions of Zr, Ti, and Misch metals provided some improvement to reduce the degradation by nucleation of favourable variants [9]. Their findings provided a window of opportunity to explore more elements as trace additions that can reduce the SMA degradation at peak aged conditions more effectively. Ti [9,22] and Zr [23] were also found to aid in grain refinement through the formation of fine compounds by reducing the amount of quenched-in vacancies and providing the opportunity for relaxation of stress concentration at the grain boundaries. Reportedly [2] this can also improve the fracture and fatigue resistance of the alloy. Xu [24] reported a significant grain refinement when Gd was added to the Cu–Zn–Al alloy but it showed no effect on the martensitic transformation. However, the composition of Cu–Zn–Al alloy in the experiments of Xu was markedly different than the present composition. Therefore, a detailed understanding of the effect of trace addition in Cu–Zn–Al alloys is proven to be an interesting topic of discussion.

Literature suggests that Sc evidently acts as a potent grain refiner in aluminium alloys [25]. Further, it has a pronounced effect on the microstructure and properties of Al alloys through the formation of the coherent Al_3Sc compound. However, such effect of Sc is not reported for Cu alloys. The presence of Al in the current alloy system makes it worthy to explore the effect of the minor addition of Sc and subsequent microstructural evolution of Cu–Zn–Al alloys.

Table 1 Average chemical composition (wt%)

Specimen name	Cu	Zn	Al	Sc
A	76.52	13.12	9.36	Nil
B	76.42	13.62	9.11	0.10

A carefully conducted literature review followed by the systematic experimental work, described in relevant sections help to understand the effect of Sc on the base alloy. It involves thermally induced phase transformations by ageing treatments. Microhardness measurements confirm the ageing response of the SMAs. Differential scanning calorimetry (DSC) experiments indicate the shape memory effect (SME) in terms of transformation temperatures. XRD analysis and microstructural evolution by optical microscopy (OM), scanning electron microscopy (SEM), and transmission electron microscopy (TEM) demonstrate the phase evolutions during ageing. The primary objective of the current research work was to investigate whether the addition of Sc brings any noticeable effect in the properties of Cu–Zn–Al alloy. Selection of only two alloy compositions helped to keep the work limited and to investigate the alloys in more detail.

2 Materials and Methods

The Cu–Zn–Al-based alloy A of nominal composition displayed in Table 1 was casted by induction melting of Cu, [70:30] brass and Al of 99.999% purity in a graphite crucible. The alloy B with 0.1% Sc was prepared by mixing Al–2%Sc master alloy with the same base alloy melt. The casts were homogenized and hot-rolled at temperature 850 °C to reduce the thickness of the strips from 8 to 2 mm. Multiple rolling passes were performed to avoid the rolling defects. Finally, the hot-rolled specimens were cut into suitable pieces for solution treatment and other experiments. The specimens were then soaked at the β-phase region, temperature 825 °C for 30 min, followed by quenching into ice-brine solution [9,22,23,26]. EDAX and spectroscopic analysis were performed to measure the quantitative compositions of the respective elements in the matrix of the specimens. The JEOL Supra 55VP made SEM was used for EDAX and spectrovac was used for spectroscopic analysis. The average of these two measurements is reported in Table 1 as the results were in the close vicinity, having 95% confidence index, the standard deviation value is approximately 2% of the reported values. Figure 2 shows the location of the spots for different specimens and chemical composition of the respective alloys measured by EDAX.

The first set of quenched specimens were subjected to DSC study using a Q 200, TA DSC instruments in the temperature range between 200 and 500 °C, with a heating and cooling rate of 10 K min^{-1}. The second set of quenched specimens were isothermally aged in a laboratory-type furnace with a resistance embedded heating cell at 300 °C for the different time interval, and the final set of quenched specimens were isochronal aged in a muffle furnace from 100 to 600 °C for 60 min. In each case, the specimens were quenched into ice-brine solution.

A Microduramet Vickers microhardness apparatus attached with Polyver Met metallograph was used for microhardness measurements. Polished specimens were subjected to hardness measurements under a constant load of 300 gmf. Every hardness data are an average of 10 measurements, and the accuracy is ±2.5 for a confidence level of 0.95. Appreciable distance has been kept between two indentations to avoid any possible cold working effect.

Crystal structures of the alloys were determined by using X-ray diffractograms taken in a Panalytical XRD by Cu–Kα radiation with a wavelength of 1.54 Å. Diffractograms with a 2θ range between 25° and 110° were indexed by comparison with the master charts. Selected specimens aged at different temperatures for 60 min with the well-polished condition were subjected to microstructural characterization using DP70-Optical, JEOL supra 55VP-SEM instruments and TECNAI, 200 kV, G2ST, FEI made TEM. TEM specimens were prepared by bringing down the thickness to 100 μm and then punching 3 mm discs out. Electropolishing was conducted using an electrolyte of 33%HNO_3 and 63%Methanol at about −20 °C with 0.8 A current and 8 V voltage in a Struers-Tenupol-3 Double Jet Electropolisher to perforate the specimen. The perforated thin foils were washed in methanol.

3 Results and Discussion

3.1 Interpretation of Equilibrium Phases Using THERMOCALC Software

A thermodynamic calculation was performed to identify the phase fractions, present at different temperatures using commercial Thermocalc [27] software in combination with TCAL5 database [28]. This is to be noted that phase prediction using Thermo-Calc is an indication and its resemblance with the XRD analysis highly depends on the Thermo-Calc database.

Figure 3a forecasts the equilibrium phases present in the base alloy Cu–Zn–Al ternary system. The low-temperature phases at quenched condition are mainly manifested by cubic phases of 1 (BCC_B2#2), 4 (γ-D83) and 6 (FCC_L12#1). The Cu–Zn binary system shows possible occurrence of CuZn and Cu_5Zn_8 ordered phases simulating the phase 1 (BCC_B2#2) and in agreement with the ordered B2 phase

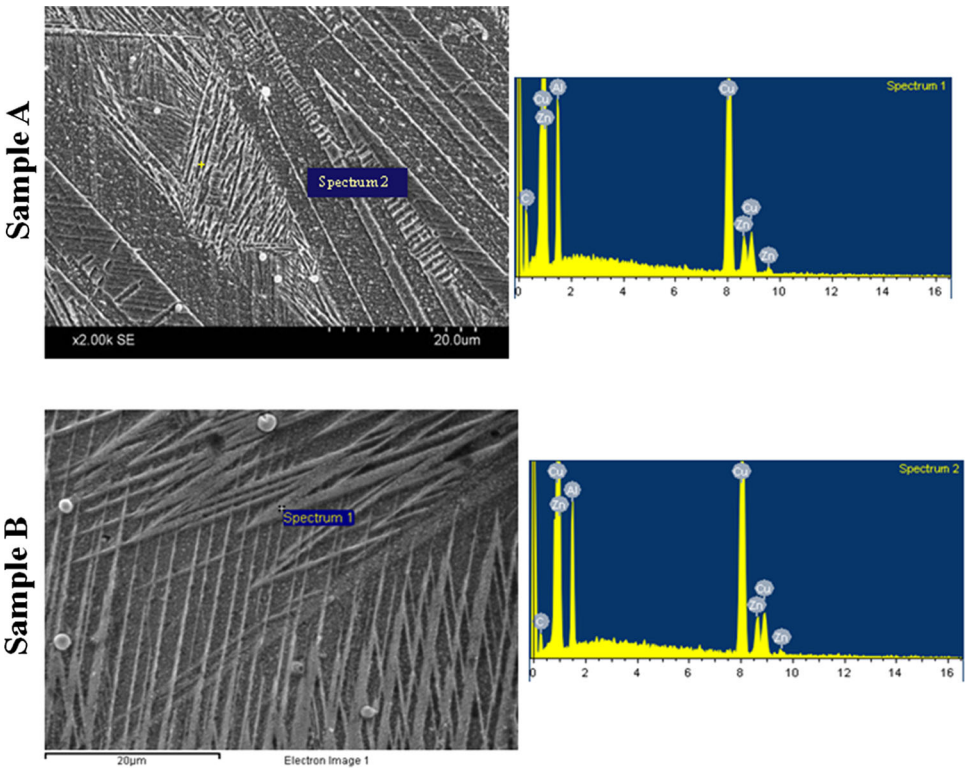

Fig. 2 SEM images showing location of spots chosen for estimation of chemical composition by EDAX

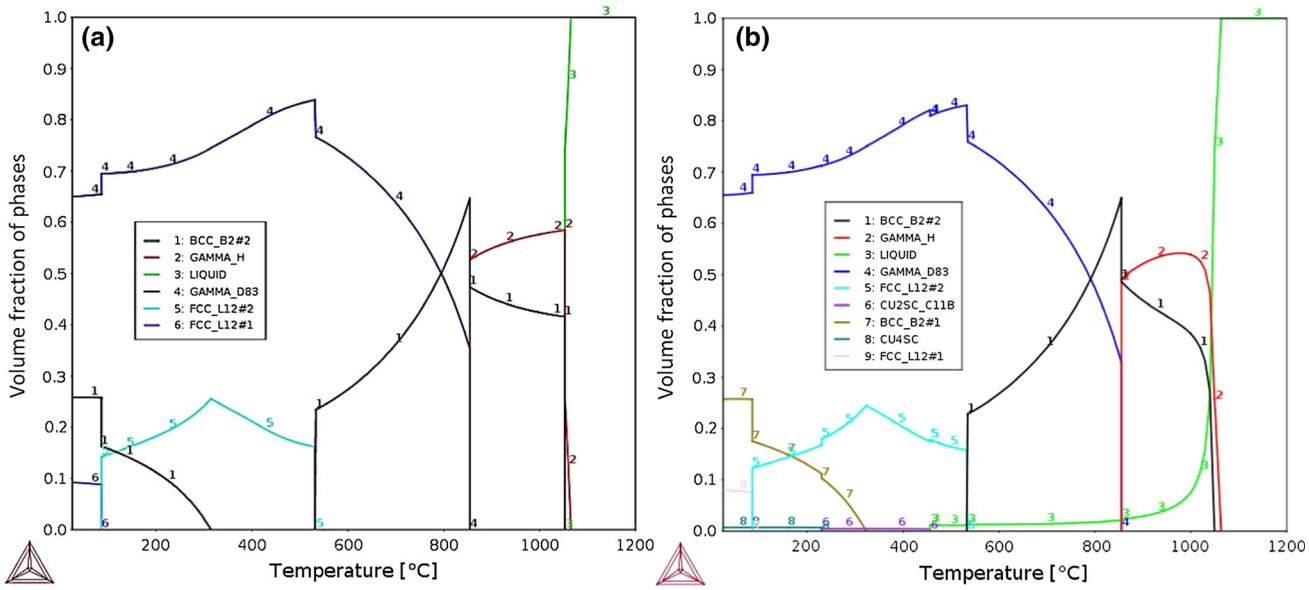

Fig. 3 Phase fraction predictions as a function of temperature by thermocalc software; **a** alloy A and **b** alloy B

shown in phase diagram (Fig. 1). The phase 6 (FCC_L12#1) is the austenitic phase indicating presence of retained austenite and correlates to the high-temperature β phase for the Cu–Zn–Al ternary system. Also, phases belong to Cu–Al binary system can be observed as 4 (γ-D83) in the diagram. The phase was identified as Cu_9Al_4 phase, having FCC structure resembling with γ-D83 phase. However, an appreciable presence of tetragonal $CuAl_2$ precipitates may present there which is difficult to distinguish from the equilibrium phase diagram. Further ageing of the alloy at the range of 200–300 °C elucidates an increase in the phase fractions of 5 (FCC_L12#2) and 4 (γ_D83) and an abrupt drop in 1 (BCC_B2#2). The database indicates that 5 (FCC_L12#2) phase is mainly the Cu-rich phases which might have the possible compositions of Cu_4 or 73%Cu–11%Al–16%Zn, both having FCC structure. The Cu–Al system consisting of

Table 2 Transformation temperatures (°C) measured from DSC for unaged conditions

Alloy	M_f	M_s	A_s	A_f
A	42	74	84	124
B	08	30	35	48

Cu_9Al_4 phase can also be observed increasing with increasing temperature. The ageing of the base alloy A at the range of 400–500 °C displays mainly the phase of 4 (γ_D83) and 5 (FCC_L12#2). The possible structure and composition of the phases have been described above.

The phase fraction as a function of temperature is presented in Fig. 3b for alloy B with 0.1% Sc. The alloy in quenched condition exhibits presence of equilibrium phases of 8 (Tetragonal Cu_4Sc), 9 (FCC_L12#1), 7 (BCC_B2#2) and 4 (γ-D83). It is most likely that a very minute quantity of tetragonal Cu_4Sc was precipitated during quenching. Similar Xs-like precipitates, for example, precipitates of Cu_2AlSc, may also form during quenching and are hard to bring in thermodynamic calculation with this software. The phase 9 (FCC_L12#1) indicates retained austenite as observed in case of alloy A and identified as 6 (FCC_L12#1). The presence of ordered phase 7 (BCC_B2#2) comparable to the phase 1 (BCC_B2#2) in alloy A can be observed that correspond to the Cu–Zn binary system. The ageing of alloy B at the range of 200–300 °C represents diminishing phases 7 (BCC_B2#2) and 8 (Tetragonal Cu_4Sc). However, phases 4 (γ-D83) and 5 (FCC_L12#2) show a reasonable increase. This is consistent with the previous case for alloy A. There is a decrease in the phase fraction of 5 (FCC_L12#2), i.e., Cu-enriched phases above 400 °C. However, phase 4 (γ-D83), i.e., phases corresponding to Cu–Al binary system shows an increasing trend. Further ageing at 500 °C indicates a sharp drop in volume fraction of the 5 (FCC_L12#2) and 4 (γ-D83) phases. XRD analysis was carried out for alloy A and B in light of thermodynamic prediction of phases to explain their evolution during ageing.

3.2 DSC Study

DSC analysis is widely used to determine the phase transformation temperatures and the latent heats during the transformation of SMAs [29,30]. In a typical DSC plot for SMAs, the transformation temperatures (M_s: start temperature of martensitic transformation; M_f: finish temperature of martensitic transformation; A_s: start temperature of austenitic transformation; A_f: finish temperature of austenitic transformation) are derived from the intersection points between the tangents to the start and end regions of the transformation peak and the baseline of the heating and cooling curves [31,32]. Transformation temperatures for present SMAs were calculated from DSC results and are presented in Table 2.

Investigation of heat-treated specimens through DSC is of general interest as the presence of different phases of different heat-treated conditions may eventually alter shape memory effect by influencing the recoverable strain [9,22,33].

Figure 4 represents DSC curves during heating and cooling for different compositions and heat-treated conditions (unaged and aged at 300 °C for 60 min). The decrease in transformation temperatures has been recorded after addition of 0.1% Sc. Tadaki et al. [2] reported that the transformation temperatures (M_s and A_s) of Cu–Zn–Al shape memory alloys are dependent on the chemical compositions. Based on this argument, alloy B should show an increase in martensite stability, similar to alloy A, which is in contrast to the observation presented in Fig. 4 and Table 2. The DSC plots in Fig. 2 reveal a sharp decrease in all the transformation temperatures in alloy B. This is possible if the interface movement between martensite and the parent phase and the growth of martensite are favoured in alloy B. Earlier, Ti was found to be an effective refiner which reduces the diffusivity of solute atoms by reducing the growth velocity of the solidified crystals [9]. Grain refinement also leads to lowering of M_s temperature in Cu–Zn–Al SMA [2]. Hence, the lowering in transformation temperatures due to the suppression of martensitic stability in alloy B can be attributed to the presence of Sc.

Thus with a minor addition of Sc (0.1%), the stability of martensite is reduced, and this observation contradicts the findings [7] of enhanced martensitic stability for similar alloys exposed under repetitive transformation cycle. The suppression of martensitic stability in alloy B, however, can be explained by exploring the fact that Sc being an effective grain refiner lowers M_s temperature [20]. Moreover, lowering of A_f and A_s gaps after minor addition reportedly [8] favour the movement of martensitic/austenite interface. Since grain refinement reportedly [2,12] reduces M_s temperatures in Cu–Zn–Al alloys, the reduced martensitic stability can be attributed to the Sc in contrast to the compositional effect.

However, interface movement can be appreciably influenced by quenched-in vacancies and/or precipitates. Chemical segregation at the internal faults of martensite for similar alloys may make martensite-to-austenite transformation sluggish and consequently increase the gap between A_f and A_s temperature. In the present investigation, Sc promotes precipitation of Al_3Sc and Xs-like precipitates in Sc-doped alloy (alloy B) at dislocations during hot rolling at β-phase temperature. XRD analysis of alloy B at quenched state confirms the Xs phase as Cu_2AlSc with cubic crystal structure [34,35]. Xs-like precipitates are formed reportedly in Ti-doped Cu–Al–Ni [20], V-doped Cu–Al–Ni–Mn high-temperature shape memory [36] alloys and Ti added Cu–Zn–Al [22] alloys. Thus, finer Xs phases retard the migration of dislocations which act as a sink for quenched-in vacancies, favouring the interface movement by dissolving the excess vacancies. However, in the base alloy (alloy A) at intermediate tem-

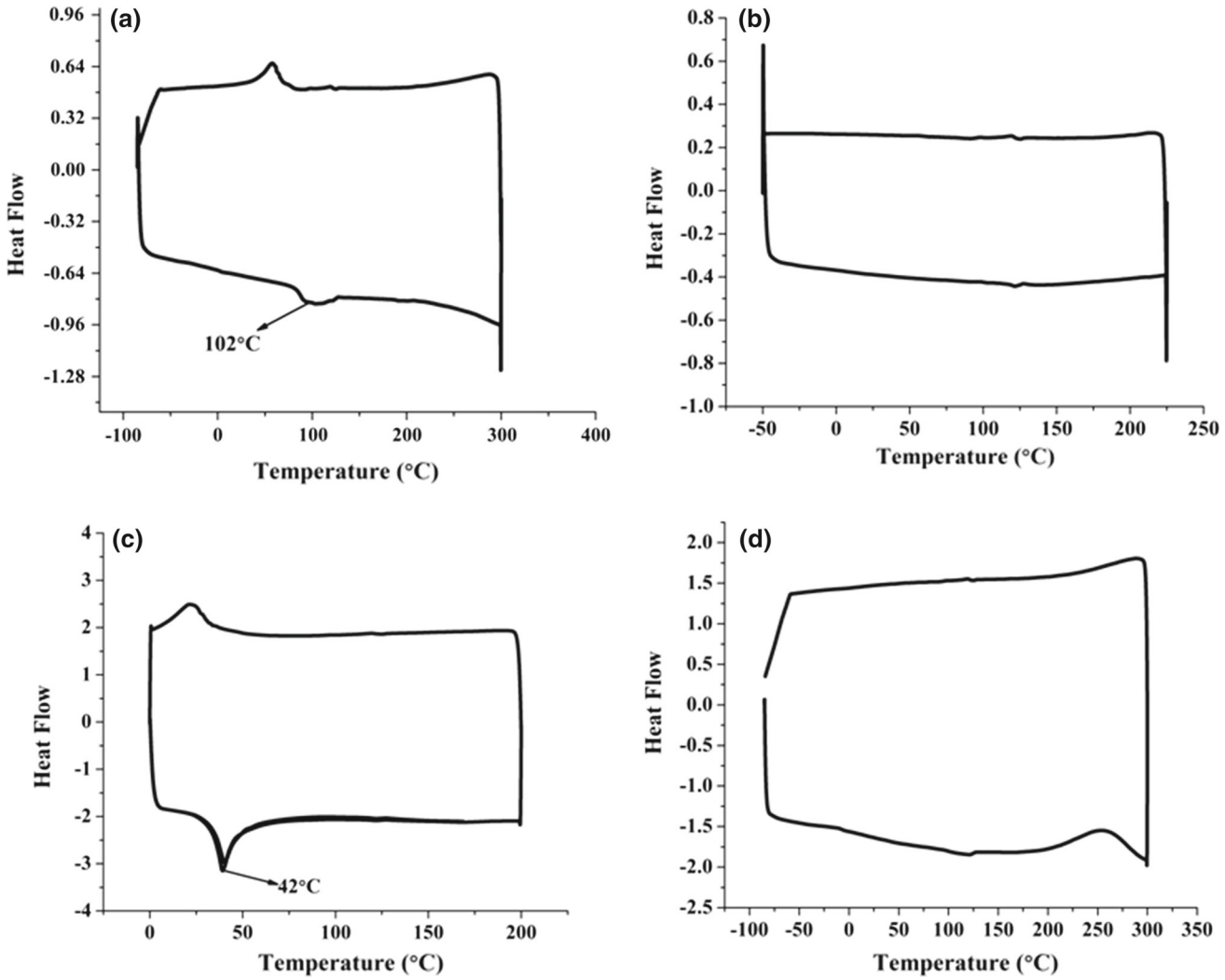

Fig. 4 DSC of investigated alloys quenched and aged at 300 °C for 60 min; **a** alloy A quenched, **b** alloy A aged, **c** alloy B quenched and **d** alloy B aged

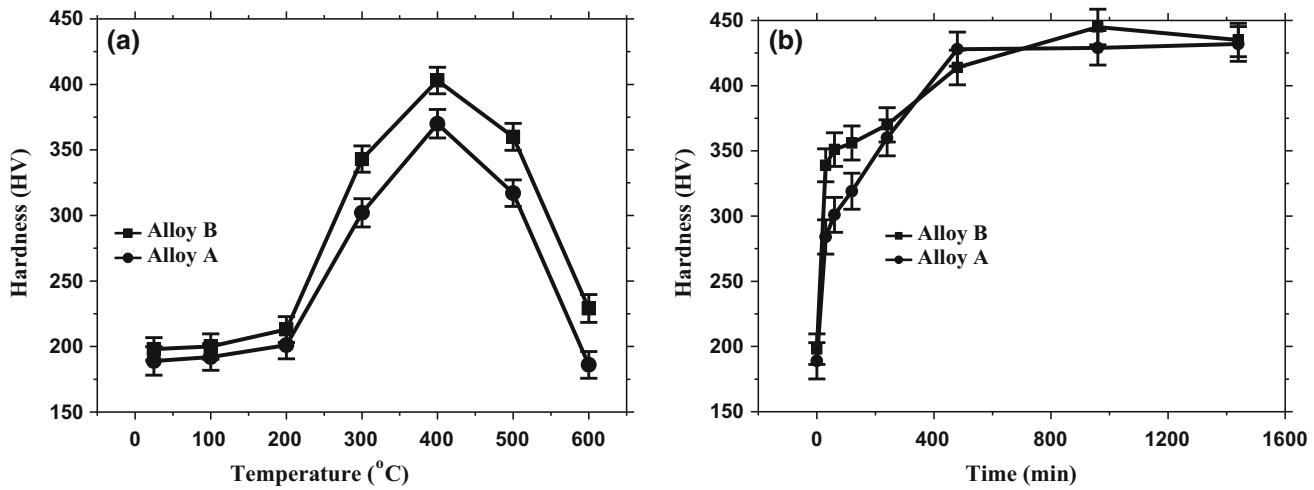

Fig. 5 Variation of hardness **a** with temperature for isochronal ageing for 60 min **b** with time for isothermal ageing at 300 °C

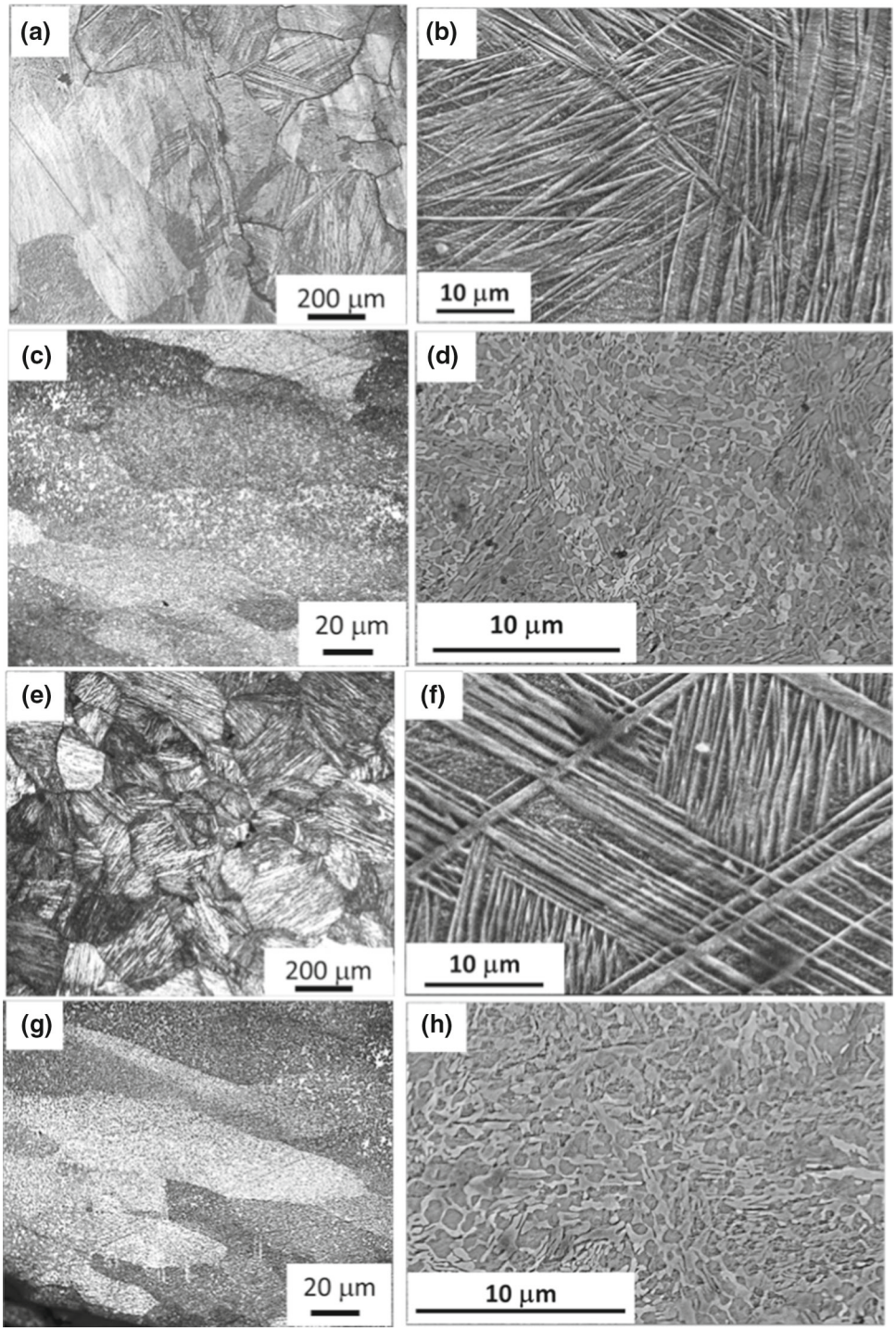

Fig. 6 Microscopy **a** and **b** unaged alloy A optical and SEM **c** and **d** aged alloy A at 400 °C for 60 min optical and SEM **e** and **f** unaged alloy B optical and SEM **g** and **h** aged alloy B at 400 °C for 60 min optical and SEM

peratures during ageing a disorder to ordering reaction takes place which annihilates the lattice defects/dislocations easily as no fine precipitates are present there to pin these dislocations. Thus no dislocations remain available to act as a sink for excess vacancies, and hence these vacancies play the major role inhibiting the martensite–austenite interface movement, which explains the higher transformation temperatures in case of alloy A than alloy B [3,13].

It may be noted that both alloys, A and B, after ageing at 300 °C for 60 min exhibited no DSC peaks depicting that complete transformation from product to parent phase occurred at this temperature. Microstructural investigation and XRD results in the following sections support this observation. This observation may be attributed to the compositional sensitivity of Cu–Zn–Al alloys [3].

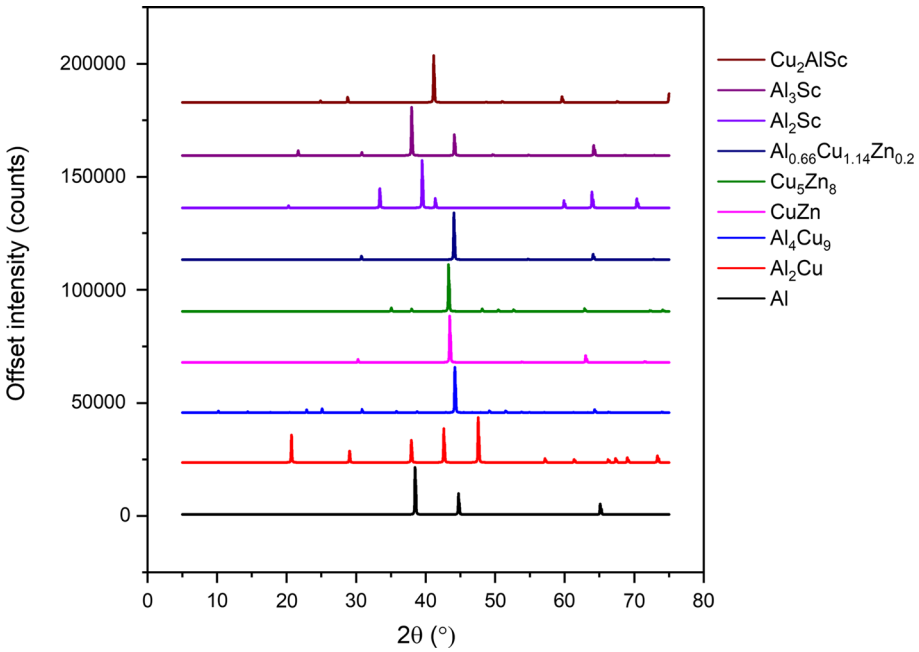

Fig. 7 Diffraction patterns of all the evolved phases for both of the alloys A and B clearly depicting corresponding intensity as a function of 2θ angles

3.3 Isothermal and Isochronal Ageing

Figure 5 shows the variation of microhardness as a function of ageing temperature and time. For isochronal ageing curves (Fig. 5a), hardness increases rapidly after 200 °C and attains a maximum at 400 °C before it goes down further. The ageing response in the case of isothermal holding hardly revealed any difference between both alloys. The hardness increased up to 400 min of holding time and exhibited a plateau thereafter.

However, isochronal ageing between 300 and 600 °C showed Sc-added alloy (B) possessing higher hardness. This observation supports Sc being a potent grain refiner.

It is important to understand the effect of ageing on the transformation temperatures of the respective alloys. The DSC plots reveal the austenitic transformation temperatures for alloy A and alloy B as 102 and 42 °C, respectively, during heating. Thus, these are the precipitate formation temperature regimes which control the microstructural evolution and corresponding shape memory behaviour of the materials. The ageing curves (Fig. 5) were found to be consistent with DSC plots in Fig. 4. The initial increment in hardness (Fig. 5b) for both alloys during ageing was occurred in almost similar precipitation temperature regimes (up to ∼ 120 °C). The ageing hardness of alloy A was attributed to the initial crystal reorientation and formation of γ_2-phase (Cu_9Al_4) and γ-phase (Cu_5Zn_8) by a diffusion mechanism. More details about the ageing behaviour are explained below with the help of microscopy and XRD results in Sects. 3.4 and 3.5.

3.4 Optical and Scanning Electron Microscopy

To investigate the effects of ageing on alloy A and B, the microstructures at room temperature was monitored by optical and scanning electron microscopy. For unaged alloys, a typical spear-head martensite morphology along with a significant presence of habit planes and favourably oriented lattice invariant twins were observed. This phenomenology is better restored in case of trace added (Fig. 6e, f) alloy (alloy B). Sc helps in nucleation of favourably oriented habit planes which reduces the shape strain in alloy B [22]. Optical micrographs of both alloys, at peak aged condition, revealed the absence of martensitic phases. Reduction in grain size in alloy B is also evident in Fig. 6 g. Thus, a higher hardness of alloy B is due to the reduction of grain size which may be a direct consequence of Sc addition. SEM micrographs for both alloys confirm the presence of complete parent phase transformation that supports the absence of any DSC peaks in aged condition (Fig. 4b for alloy A and 4d for alloy B).

3.5 X-ray Diffraction

XRD analysis of all the plausible phases had been conducted for alloys A and B from their quenched condition to the ageing temperature at 500 °C. The intensity counts of the evolved phases for both the alloys are shown in Fig. 7 as a function of 2θ angles. Table 3 clearly demonstrates the reflection planes to the corresponding 2θ angles of each phase identified by XRD. The patterns provided in Fig. 7 evidently supports the XRD analysis made in the subsequent section. A detailed discussion is given below explaining the DSC, ageing curves

Table 3 Reflection planes with corresponding 2θ angle for each phase

	h	k	l	2θ (°)
$Cu_{4.00}$	1	1	1	42.466
	0	0	2	49.44
	0	2	2	23.00
	1	1	3	87.813
Al	1	1	1	38.48
	2	0	0	44.73
	3	1	1	78.248
$Cu_{1.14}Zn_{0.20}Al_{0.66}$	1	1	0	44.064
	2	0	0	64.08
	2	1	1	81.044
Al_2Cu	1	1	2	42.612
	3	1	0	47.50
	2	2	2	57.168
	4	0	2	73.329
	0	0	4	78.306
	3	2	3	82.352
	5	2	1	88.898
	5	1	2	92.093
	3	1	4	96.811
Al_4Cu_9	3	3	0	44.209
	4	2	1	47.963
	6	3	3	81.348
	7	4	1	92.199
Cu_2AlSc	2	2	0	41.154
	4	2	2	74.99
	4	4	0	89.325
Al_2Sc	3	1	1	39.492
	2	2	2	41.384
	4	4	0	70.359
Al_3Sc	1	1	1	37.972
	2	0	0	44.131
	3	1	1	77.066
Cu_5Zn_8	3	3	0	43.298
	3	3	2	48.131
	6	0	0	62.884
	4	4	4	74.078
	7	2	1	79.417

and microstructures in light of the evolved phases of the corresponding alloys at respective ageing condition.

XRD of alloy A at unaged and aged at 200, 400 and 500 °C for 60 min are shown in Fig. 8. On quenching from betatizing temperature to the temperature of ice-brine solution, martensitic transformation (β_1' phase) can be viewed by optical and scanning electron micrographs (Fig. 6a, b). XRD analysis was used to determine the nonstoichiometric composition as $Al_{0.66}\,Cu_{1.14}Zn_{0.2}$. There are also peaks for the solid solution of aluminium in copper γ_2-phase (Al_4Cu_9) and Tetragonal Al_2Cu superstructure. Peaks of γ- cubic phase was identified as Cu–Zn compositions mainly precipitates of Cu_5Zn_8. The analysis is in good agreement with Thermo-Calc calculations which predicted presence of 1 (BCC_B2#2) and 4 (γ-D83) phases. It is reported [37] that slow cooling rate produces α and $\gamma_2$phases significantly whereas quenching mainly produces β_1' phase. Although the evolution of phases strongly depends on compositions [13,37].

Alloy A after ageing at 200 °C mainly exhibited reorientation of crystal structure, disordered β_1' phase transforms to ordered β_1 phase [37–39] consistent with ordered B2 phase-1 in Thermo-Calc calculations. Since long the "stabilization of martensite" has been considered as the most attractive metallurgical behaviour that occurs in this temperature region, to explain the shape memory behaviour. Ren and Otsuka [16,17] explained the stabilization mechanism by conforming short-range order. Castro and Romero reported decomposition of β phase during martensitic ageing of Cu–Zn–Al alloy in bainitic phase and cuboidal precipitate at 603 K [40]. Ahlers and Pelegrina [41] explained Cu–Zn–Al martensite stability on long-range ordering (LRO) mechanism and to some extent on short-range ordering (SRO). During ageing below M_s temperature, it was found that A_s and A_f temperatures rise thus preventing reversion of martensite back into parent phase upon heating. Stabilization of martensite in directly quenched condition is enhanced by high concentration of quenched-in vacancies. This is also influenced by composition, grain size and crystal defects [13]. Fine-grained material might be recognized less susceptible to stabilization due to a higher proportion of grain boundaries those act as effective sinks for vacancies, mitigating their contribution to diffusion [36]. XRD results at 200 °C ageing may be explained by this phenomenon where phases are almost identical with quenched conditions. Some partial diminishing/overlapping and evolution of peaks are attributed to the reorientation in crystal structures due to diffusion. The result is further supported by the hardness data both from isothermal and isochronal ageing where the increase in hardness was found to be very low.

Further, isochronal ageing at 300 °C for 60 min show enhancement of hardness which may be attributed to the formation of α-phase, mainly Cu-enriched phases shown as 5 (FCC_L12#2). DSC study (Fig. 4b) at 300 °C revealed no peak formation, elucidating completion of austenitic transformation from martensite at 300 °C. The result is consistent with the isothermal ageing result. Further ageing isothermally after 10 h for both alloys resulted in linear hardness values depict that both alloys are quite sensitive to temperature that provides the driving force for phase transformations, supported by isochronal ageing at 400 °C for 60 min.

The peak aged alloy at 400 °C represents clear austenitic transformation with an appreciable presence of γ-phase (Al_4Cu_9). Optical and SEM shown in Fig. 6c, d revealed

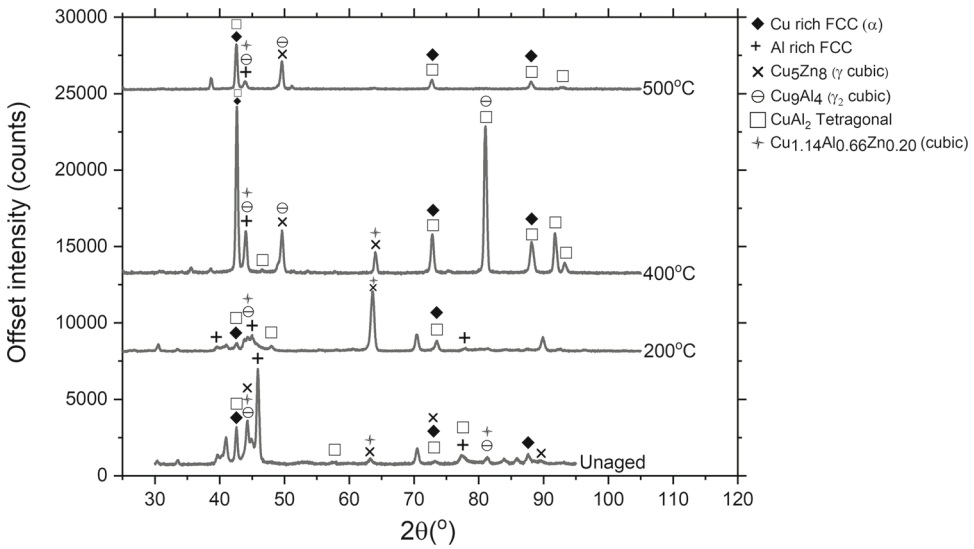

Fig. 8 XRD of alloy A quenched and aged at 200, 400, and 500 °C for 60 min

austenitic microstructure and complete absence of martensitic grain. Similar precipitations of γ-phase were reported during ageing of Cu–Zn–Al alloy with higher Al content [42–45]. The higher value of hardness can be attributed to the presence of γ-phase which is in a good deal with [13,46].

Ageing of alloy A at 500 °C resulted in partial restoration of austenitic β phase. Minor presence of γ-phase (Al_4Cu_9) indicated dissolution of these precipitates to the parent matrix. This also leads to a decrease in hardness assisted with a loss of coherency [13] and grain coarsening when aged at 500 °C for 60 min.

The DSC plots shown in Fig. 4 revealed a sharp decrease in M_s temperature in the case of Sc bearing alloy (alloy B) which contradicts the effect of compositional variation on M_s temperature in Cu–Zn–Al SMA, established by Tadaki [2,3]. Thus the favoured interface movement of martensite/parent phase may be attributed to the direct consequence of Sc effect, which reduces the diffusivity of solute atoms and acts as potent grain refiner [47–49] lowering M_s temperature [3] that results compromising of martensite stability. A similar observation was reported in case of Ti addition in Cu-bearing alloys by Adachi [20] and Bhuniya et al. [22].

The XRD analysis (Fig. 9) of alloy B in quenched condition proved the presence of Cu_2AlSc-like precipitates in contrast to the precipitates of tetragonal Cu_4Sc as predicted by Thermo-Calc software. Such discrepancies can be attributed to the databases used for the respective analysis. The presence of Cu_2AlSc demonstrates that these are the Xs-like precipitate phases earlier reported in Ti [20] and V [3] added Cu–Al–Ni and Cu–Zn–Al alloys, respectively, which might be formed during hot rolling at β-phase temperature. These precipitates formed preferentially at the dislocation originated during hot rolling, retained the dislocations in quenched state and did not dissolve at betatizing temperature [22]. It was also reported that Xs phase hardly capable of pinning the martensite/austenite interface [22]. Thus the dislocations play as sinks of quenched-in vacancies, formed during quenching in martensitic microstructure [3]. Thus, it does not hinder the martensite/parent interface movement, whereas in case of alloy A, the absence of Xs-like precipitates favours the annihilation of dislocations during betatizing, and thus the quenched-in vacancies play an active role by hindering the interface movement causing martensitic stability. The presence of Cu_2AlSc like precipitates is evident in Fig. 9 for unaged and aged alloy B at 200 °C.

On further ageing at 400 °C, depletion of Al atoms occurs from the matrix due to the higher affinity of Al towards Sc rather Cu. Thus, the proportion of Al_3Sc phases is generated in the expense of dissolution of Al_4Cu_9 and Cu_2AlSc phases. Since Al_3Sc precipitates have a more effective pinning effect [41], therefore alloy B exhibits higher hardness (Fig. 5a). This is also supported by the lower grain size shown in Fig. 6 g. The rest of the ageing behaviour of alloy B at 500 °C is comparable to that of the alloy A. Since the alloy gets overaged, a decrease in hardness is eminent as particle-coarsening effect.

3.6 Transmission Electron Microscopy

Figure 10 exhibits the TEM bright-field images with corresponding SAD pattern of alloy A and B for the purpose of comparing the role of Sc on the microstructure for peak aged condition (400 °C). The bright-field TEM micrographs were recorded near the [001] incident beam and the corresponding selected area diffraction (SAD) patterns were recorded to [001] zone axes. TEM image and SAD patterns of sample A (Fig. 10) revealed an apparent number of dislocations and nano sized precipitates (mainly Cu–Zn) in the Cu matrix. The presence of nanosized precipitates has been identified by many researchers [50]. The precipitates became finer after addition of Sc as depicted from the bright-field and SAD

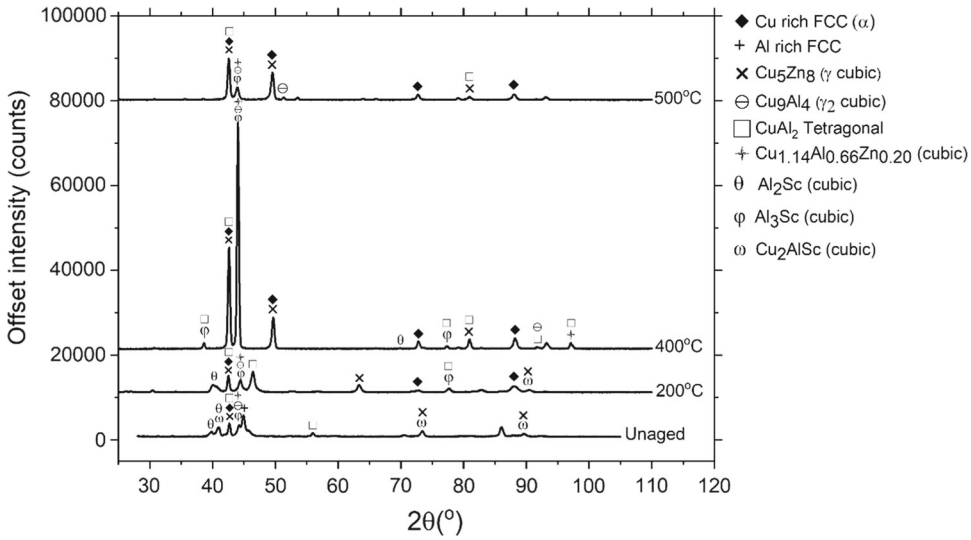

Fig. 9 XRD of alloy B quenched aged at 200, 400, and 500 °C for 60 min

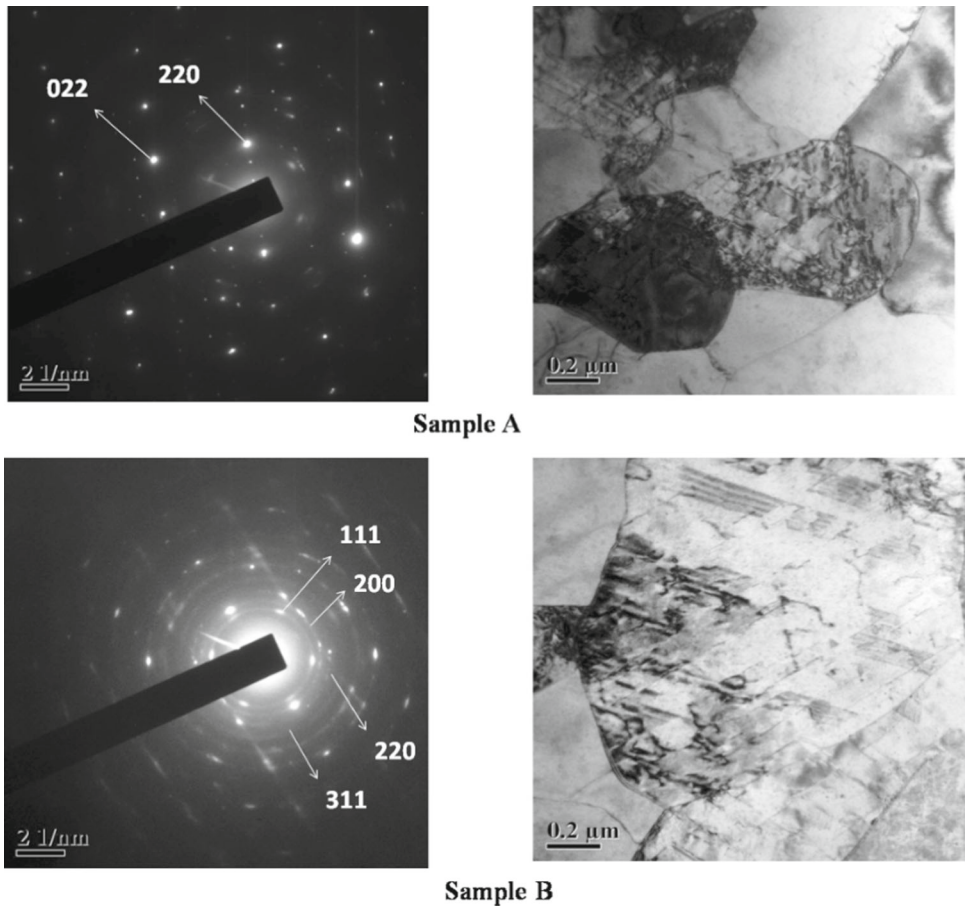

Fig. 10 TEM bright-field images with corresponding SAD patterns for alloy A and alloy B for [001] zone axis

pattern being circular in appearance. The change has also been noticed in shape and nature of the precipitates. Most of the precipitates in alloy B are lath in shape compared to circular in alloy A, as corroborated in the SAD pattern owing to the deviation in spot shape. Al_3Sc became the majority of the precipitates due to greater affinity of Sc towards Al [51]. Al_3Sc exhibits FCC structure, have high melting point, good heat endurance and homogeneous distribution throughout the matrix. Presence of Al_3Sc efficiently explains greater hardness for alloy B during isochronal ageing (Fig. 5). The Al_3Sc precipitates play an important role while they interact with dislocations making proliferation of Frank–Read and the substructure strengthening as two active strengthening mechanisms. Interestingly, addition of Sc increased

twinned microstructure in alloy B. Twining being promoted by low stacking fault energy (SFE) and consequently inhibiting cross-slip, Sc presumably played a major role. Lowering of SFE due to addition of Sc is possibly responsible for generation of twining in alloy B. Presence of "tweed" contrast spots in SAD of specimen A demarcates presence of twining and further corroborated in the bright-field image of specimen B.

4 Conclusions

The present study aims to understand the effect of tracer Sc in Cu–Zn–Al shape memory alloys. The two compositions without Sc and 0.1% Sc were subjected to isothermal and isochronal ageing. The ageing response of the alloys was analysed using advanced characterization techniques and the following conclusions were drawn;

1. The composition without Sc displayed the well-known "martensitic stability" which is typical for similar kind of alloys and attributed to the reduced mobility of martensite–austenite interface. However, the tracer addition of Sc exhibited a significant reduction in transformation temperature indicating an increase in mobility of the martensite–austenite interface. This reduces the degradation of shape memory effect (SME) during repetitive transformation cycling at a lower temperature range.
2. The martensite–austenite interface migration is hindered by the quenched-in vacancies in case of alloy A. But XRD results reveal the evolution of Cu_2AlSc precipitates in case of alloy B at the quenched condition and to some extent at 200 °C. The precipitates pin the dislocations generated during hot rolling and these dislocations sink the quenched in vacancies favouring the migration of martensite–austenite interface. This suppresses the martensitic stability and results in reduced transformation temperature. The Cu_2AlSc precipitates form favourable variants in Sc-added alloy, minimizing the degradation of shape memory effect (SME) during repetitive transformation cycling.
3. Sc addition acts as potent grain refiner by producing finer precipitates increasing the hardness of the alloy.
4. The peak hardness of the alloy A is attributed to the formation of Al_4Cu_9 phase whereas Al_3Sc precipitates increase the hardness of alloy B delineating effective pinning effect.
5. TEM results confirm the presence of finer precipitates and significant twining in alloy B.

Acknowledgements We sincerely thank Dr. D.Y. Cong, Prof. M.R. Barnett, and Prof. M. K Banerjee for providing their significant insight and expertise that greatly assisted the research.

References

1. Stalmans, R.; Humbeeck, J.V.; Delaey, L.: Degradation of the shape-memory effect in copper-base alloys. Scr. Metall. Mater. **31**(11), 1573–1576 (1994)
2. Otsuka, K.; Wayman, C.M.: Mechanism of shape memory effect and superelasticity. In: Otsuka, K., Wayman, C.M. (eds.) Shape Memory Materials, pp. 27–48. Cambridge University Press, Cambridge (1998)
3. Tadaki, T.; Otsuka, K.; Shimizu, K.: Shape memory alloys. Ann. Rev. Mater. Sci. **18**(1), 25–45 (1988)
4. Asanović, V.; Delijić, K.; Jauković, N.: A study of transformations of β-phase in Cu–Zn–Al shape memory alloys. Scr. Mater. **58**(7), 599–601 (2008)
5. Funakubo, H.: Shape Memory Alloys. Taylor & Francis, Milton Park (1987)
6. Dasgupta, R.; Jain, A.K.; Kumar, P.; Hussein, S.; Pandey, A.: Effect of alloying constituents on the martensitic phase formation in some Cu-based SMAs. J. Mater. Res. Technol. **3**(3), 264–273 (2014)
7. Bhattacharya, S.; Bhuniya, A.; Banerjee, M.K.: Influence of minor additions on characteristics of Cu–Al–Ni alloy. Mater. Sci. Technol. **9**(8), 654–658 (1993)
8. Bruke, R.J.: In: Wang, F.F.Y. (ed.) Ceramic Fabrication Processes, p. 331. Academic Press, New York (1976)
9. Bhuniya, A.K.; Datta, S.; Chattopadhyay, P.P.; Banerjee, M.K.: Effect of trace addition on the microstructural degradation of Cu–Zn–AI shape memory alloy. In: Proceedings of Seminar on Resurgence of Metallic Materials the Current Scenario (ROMM-2002), 24–25 Oct 2002. National Metallurgical Laboratory(CSIR), Jamshedpur (2002)
10. Miyazaki, S.; Otsuka, K.: Development of shape memory alloys. ISIJ Int. **29**(5), 353–377 (1989)
11. Delaey, L.; Deruyttere, A.; Aernoudt, N.; Roos, J.R.: Shape Memory Effect, Super-Elasticity and Damping in Cu–Zn–Al Alloys. INCRA Research Report (Project No. 238), Feb 1978
12. Otsuka, K.; Wayman, C.M.: Shape Memory Materials. Cambridge University Press, Cambridge (1999)
13. Tarhan, E.: Ageing characteristics of copper based shape memory alloys. Ph.D. Dissertation, The Middle East Technical University (2004)
14. Miyazaki, S.; Otsuka, K.: In: Funakubo, H. (ed.) Shape Memory Alloys, p. 116. Gordon and Breach Science Publishers, Philadelphia (1984)
15. Tarhan, E.: Ageing characteristics of copper based shape memory alloys. Thesis (2004)
16. Otsuka, K.; Ren, X.: Mechanism of martensite aging effect. Scr. Mater. **50**(2), 207–212 (2004)
17. Otsuka, K.; Ren, X.: A comparative study of elastic constants of Ti–Ni-based alloys prior to martensitic transformation. Mat. Sci. Eng. **A312**, 196–206 (2001). https://doi.org/10.1016/S0921-5093(00)01876-1
18. Ahlers, M.; Pelegrina, J.L.: Ageing of martensite: stabilisation and ferroelasticity in Cu-based shape memory alloys. Mater. Sci. Eng. A **356**(1–2), 298–315 (2003)
19. Guilemany, J.M.; Gill, F.J.: Kinetic grain growth in Cu-Zn-Al shape memory alloys. J. Mater. Sci. **26**, 4626 (1991). https://doi.org/10.1007/BF00612397
20. Adachi, K.S.K.; Hamada, Y.: Formation of (X) phases and origin of grain refinement effect in Cu–Al–Ni shape memory alloys added with titamium. ISIJ Int. **29**, 378–387 (1989)

21. Gil, F.J.; Guilemany, J.M.: Effect of cobalt addition on grain growth kinetics in Cu–Zn–Al shape memory alloys. Intermetallics **6**(5), 445–450 (1998)
22. Bhuniya, A.K.; Chattopadhyay, P.P.; Datta, S.; Banerjee, M.K.: On the degradation of shape memory effect in trace Ti-added Cu–Zn–Al alloy. Mater. Sci. Eng. A **393**(1–2), 125–132 (2005)
23. Bhuniya, A.K.; Chattopadhyay, P.P.; Datta, S.; Banerjee, M.K.: Study on the effect of trace zirconium addition on the microstructural evolution in Cu–Zn–Al shape memory alloy. Mater. Sci. Eng. A **391**(1–2), 34–42 (2005)
24. Xu, J.W.: Effects of Gd addition on microstructure and shape memory effect of Cu–Zn–Al alloy. J. Alloys Compd. **448**(1–2), 331–335 (2008)
25. Røyset, J.; Ryum, N.: Scandium in aluminium alloys. Int. Mater. Rev. **50**(1), 19–44 (2005)
26. Datta, S.; Bhunya, A.; Banerjee, M.K.: Two way shape memory loss in Cu–Zn–Al alloy. Mater. Sci. Eng. A **300**(1–2), 291–298 (2001)
27. Sundman, B.; Jansson, B.; Andersson, J.-O.: The thermo-calc databank system. Calphad **9**(2), 153–190 (1985)
28. Thermo-calc thermodynamic equilibrium calculations. Thermo-Calc Software, Stockholm. http://www.thermocalc.com/thermocalc.com/media/19849/tcal5_extended_info.pdf. Accessed 5 Aug 2018
29. Deltell, A.; Escoda, L.; Saurina, J.; Suñol, J.J.: Martensitic transformation in Ni–Mn–Sn–Co heusler alloys. Metals **5**(2), 695–705 (2015)
30. Petalis, P.; Makris, N.; Psarras, G.C.: Investigation of the phase transformation behaviour of constrained shape memory alloywires. J. Thermal Anal. Calorim. **84**(1), 219–224 (2006)
31. Cong, D.Y.; Saha, G.; Barnett, M.R.: Thermomechanical properties of Ni–Ti shape memory wires containing nanoscale precipitates induced by stress-assisted ageing. Acta Biomater. **10**(12), 5178–5192 (2014)
32. Lagoudas, D.C.: Shape Memory Alloys: Modeling and Engineering Applications. Springer, New York (2008)
33. Dasgupta, R.; Jain, A.K.; Kumar, P.; Hussain, S.; Pandey, A.: Role of alloying additions on the properties of Cu–Al–Mn shape memory alloys. J. Alloys Compd. **620**, 60–66 (2015)
34. Dwight, A.E.; Kimball, C.W.: ScT2X and LnT2X compounds with the MnCu2al-type structure. J. Less Common Met. **127**, 179–182 (1987)
35. Pisch, A.: Al–Cu–Sc (aluminium–copper–scandium). In: Effenberg, G., Ilyenko, S. (eds.) Light Metal Systems, Part 2, pp. 1–8. Springer, Berlin (2005)
36. Gao, Y.; Zhu, M.; Lai, J.K.L.: Microstructure characterization and effect of thermal cycling and ageing on vanadium-doped Cu–Al–Ni–Mn high-temperature shape memory alloy. J. Mater. Sci. **33**(14), 3579–3584 (1998)
37. Kwarciak, J.: Phase transformations in Cu–Al and Cu–Zn–Al alloys. J. Thermal Anal. Calorim. **31**(3), 559–566 (1986)
38. Occampo, G.: Sur la décomposition thermique après trempe de laβ phase de l'alliage Cu–10.1%Al–influence du nickel et du fer. Thesis, Paris (1980)
39. Greninger, A.B.: The martensite transformation in beta copper-aluminium alloys. AIME Trans. **133**, 204–227 (1939)
40. Castro, M.L.; Romero, R.: Isothermal γ precipitation in a β Cu–Zn–Al alloy. Mater. Sci. Eng. A **255**(1–2), 1–6 (1998)
41. Ahlers, M.; Pelegrina, J.L.: Ageing of martensite: stabilisation and ferroelasticity in Cu-based shape memory alloys. Mater. Sci. Eng. A **356**(1–2), 298–315 (2003)
42. Seguí, C.; Cesari, E.: Characteristics of martensite stabilization in a high temperature Cu–Zn–Al alloy. J. Phys. IV **5**(C8), C8-835–C8-840 (1995)
43. Leu, S.S.; Hu, C.T.: The aging effect on Cu–Zn–Al shape memory alloys with low contents of aluminum. MTA **22**(1), 25–33 (1991)
44. Kwarciak, J.; Bojarski, Z.; Morawiec, H.: Phase transformation in martensite of Cu–12.4% Al. J. Mater. Sci. **21**(3), 788–792 (1986)
45. Leu, S.S.; Hu, C.T.: Effect of aluminum content on precipitation in Cu–Zn–Al shape memory alloys, pp. 593–598. Referred, In: Shuchuan, C., Hsu, T.Y, Fan, Y., Jihau, Z. (eds) Stabilization of Martensite and Ordering of the Parent Phase in a CuZnAl Alloy, Proceedings of ICOMAT-92, Monterey, USA 20–24 July 1992, Perkins, J. (ed.), pp. 599–604. Monterey Institute for Advanced Studies, Monterey (1993)
46. Kayali, N.; Ozgen, S.; Adiguzel, O.: The influence of ageing on martensite morphology in shape memory CuZnAl alloys. J. Phys. IV **07**(C5), C5-317–C5-322 (1997)
47. Wong, M.J.: Development of precipitation hardenable Al–Sc–Zr–Hf quaternary alloys through thermodynamic modeling, and room-temperature and elevated temperature hardness. ME Thesis, Michigan Technological University (2014)
48. Fan, Y.: Precipitation strengthening of aluminum by transition metal aluminides. ME Thesis, Worcester Polytechinc Institute (2012)
49. Kaiser, M.: Effect of trace scandium addition on Al-6 mg alloy. J. Mech. Eng. **36**, 12–17 (2006)
50. Pons, J.; Portier, R.: Accommodation of γ-phase precipitates in CuZnAl shape memory alloys studied by high resolution electron microscopy. Acta Mater. **45**, 2109–2120 (1997)
51. Sen, R.; Ghosh, M.; Kaiser, M.S.: Microstructure-texture-fracture toughness property correlation in annealed Al-6 Mg alloy with minor scandium and zirconium additions. Fatigue Fract. Eng. Mater. Struct. **35**, 1071–1078 (2012)